A multi-species collisional operator for full-F global gyrokinetics codes : Numerical aspects and validation with the GYSELA code

Peter Donnel, Xavier Garbet, Yanick Sarazin, Virginie Grandgirard, Yuuichi Asahi, Nicolas Bouzat, Elisabetta Caschera, Guilhem Dif-Pradalier, Charles Ehrlacher, Philippe Ghendrih, et al.

A multi-species collisional operator for full-F global gyrokinetics codes : Numerical aspects and validation with the GYSELA code

P. Donnel, X. Garbet, Y.Sarazin, V.Grandgirard, Y.Asahi, N.Bouzat, E.Caschera, G. Dif-Pradalier, C.Ehrlacher, P.Ghendrih, C.Gillot, G.Latu, C. Passeron

CEA, IRFM, Saint-Paul-lez-Durance, F-13108, France

Abstract

A linearized multi-species collision operator valid for arbitrary masses and charges has been developed and implemented in the gyrokinetic code GYSELA [9]. This operator has all the required properties : it conserves particles, total momentum and energy, fulfills the Boltzmann H theorem and recovers neoclassical results. This operator takes into account both pitch angle scattering and energy diffusion while operting in the $\left(v_{\|}, \mu\right)$ phase space. Derivatives with respect to the magnetic moment are treated using a projection on a set of orthogonal polynomials. The numerical aspects of the implementation are detailed and a set of physical benchmarks allows a verification of the properties of the operator.

Keywords: collision, multispecies, H-theorem, neoclassic

1. Introduction

The perpendicular transport in core fusion plasmas is dominated by turbulent processes. Nevertheless, accounting for collisions remains essential for several reasons. First, to a large extent, collisions govern the level of large scale flows – both the mean ion poloidal flow and turbulence-driven zonal flows – via the friction on trapped particles. Second, neoclassical transport can reveal dominant (or at least competitive) with respect to turbulent transport in certain regimes such as transport barriers, or for certain classes of particles such as heavy impurities like tungsten. Third, collisions are essential for trapped electron which are often in a collisionnal regime. Finally, and more fundamentally, collisions ensure the relaxation of the distribution function towards a Maxwellian. In turn, they are critical for gyrokinetic simulations since they smooth out small scale structures in velocity space, contributing to numerical stability.

The full collision operator and its properties are well known but its non linear character makes it impossible to use numerically with present gyrokinetic codes. It is then necessary to develop a linearized model of collision operator easier to handle numerically. Different model operators have been developed in the literature [1, 17, 10, 13]. Depending on its specificity, each code chooses a different model. A PIC code like ORB5 [19] uses a different operator than an Eulerian code like GENE [18] , GKW [15] or GS2 [2]. In the framework of the GYSELA code, one of the major difficulties is to write an operator in the variables $\left(v_{\|}, \mu\right)$ whereas the collision operator is separable in the set of variables $\left(v, \frac{v_{\|}}{v}\right)$. This difficulty has been overcome by Esteve et al. in [7]. The collision operator is linearized around unshifted Maxwellians and is gyroaveraged using the method developed by Brizard [3]. It is valid for arbitrary species and can be shown to fulfill all properties required for a model collision operator. Its derivation and analytical validation can be found in details in [7]. A simplified version of this operator has been implemented in GYSELA and benchmarked against neoclassical theory [8]. It uses the slow limit approximation (energy and pitch-angle scattering are assumed equal) and removes all μ derivatives. A particular consequence of these approximations is that the implemented model is only valid for trace thermal impurities. This article describes the treatement of the collision operator without those two assumptions, hence alleviating the former restrictions regarding the domain of validity.

The outline is the following. In part II we recall the important results of the model derived by Esteve et al in [7]. Part III is dedicated to the numerical implementation of the collision operator. Part IV consists in a serie of tests which validate the collision operator.

2. Presentation of the model

The model described here is derived directly from [7]. The linearized collisional operator describing the collisions of species a colliding on species b takes the form

$$C_{ab}(F_a, F_b) = C^0_{ab}(F_{M0a}, F_{M0b}) + C^1_{ab}(F_a, F_b)$$

where F_{M0a} represents the local unshifted Maxwellian with density n_a and temperature T_a

$$F_{M0a}(\boldsymbol{x}, \boldsymbol{v}, t) = n_a(\boldsymbol{x}, t) \left(\frac{1}{2\pi v^2_{Ta}}\right)^{3/2} \exp\left(-x_a^2\right)$$

The normalized speed has been used $x_a = \frac{v}{\sqrt{2} v_{Ta}}$,with $v_{Ta} = \sqrt{\frac{T_a}{m_a}}$ the thermal velocity.

*Corresponding author.
E-mail address: peter.donnel@cea.fr

C^0_{ab} represents the exchange of energy between the unshifted Maxwellians

$$C^0_{ab}(F_{M0a}, F_{M0b}) = \frac{T_b - T_a}{T_b} x_a^2 \nu_{E,ab} F_{M0a}$$

Neglecting all finite Larmor radius effects, C^1_{ab} is composed of three terms

$$C^1_{ab}(F_a, F_b) = C_{v,ab}(F_a) + C_{d,ab}(F_a) + C_{\parallel,ab}(F_a, F_b)$$

$C_{v,ab}$ is an operator acting on the norm of the velocity. When written in the set of variables $(v_\parallel, v_\perp)$, it reads as follows:

$$\begin{aligned} C_{v,ab}(F_a) &= \frac{1}{2v_\perp}\frac{\partial}{\partial v_\perp}\left[F_{M0a}\nu_{v,ab}v_\perp^2\left(v_\perp\frac{\partial g_{ab}}{\partial v_\perp} + v_\parallel\frac{\partial g_{ab}}{\partial v_\parallel}\right)\right] \\ &+ \frac{1}{2}\frac{\partial}{\partial v_\parallel}\left[F_{M0a}\nu_{v,ab}v_\parallel\left(v_\perp\frac{\partial g_{ab}}{\partial v_\perp} + v_\parallel\frac{\partial g_{ab}}{\partial v_\parallel}\right)\right] \end{aligned}$$

Whereas $C_{d,ab}$ modifies the direction of the velocity vector (deflection)

$$\begin{aligned} C_{d,ab}(F_a) &= \frac{1}{2v_\perp}\frac{\partial}{\partial v_\perp}\left[F_{M0a}\nu_{d,ab}v_\perp v_\parallel\left(v_\parallel\frac{\partial g_{ab}}{\partial v_\perp} - v_\perp\frac{\partial g_{ab}}{\partial v_\parallel}\right)\right] \\ &+ \frac{1}{2}\frac{\partial}{\partial v_\parallel}\left[F_{M0a}\nu_{d,ab}v_\perp\left(-v_\parallel\frac{\partial g_{ab}}{\partial v_\perp} + v_\perp\frac{\partial g_{ab}}{\partial v_\parallel}\right)\right] \end{aligned}$$

Finally the term $C_{\parallel,ab}$ ensures momentum exchange between species and the conservation of the total parallel momentum.

$$C_{\parallel,ab}(F_a, F_b) = -\frac{\nu_{s,ab}(v)}{v_{Ta}^2} v_\parallel \left(U_{\parallel d,a} - U_{\parallel ba}\right) F_{M0a}$$

The normalized distribution function has to be shifted to ensure that $C_{v,ab}$ and $C_{d,ab}$ conserve momentum and energy

$$g_{ab} = f_a - \frac{v_\parallel U_{\parallel d,a}}{v_{Ta}^2} - x_a^2 q_{ba} \text{ with } f_a = \frac{F_a}{F_{M0a}}$$

More specifically, $U_{\parallel d,a}$ ensures that $C_{v,ab}$ and $C_{d,ab}$ conserve momentum.

$$\frac{v}{v_{Ta}^2} U_{\parallel d,a}(v) = \frac{3}{2}\int d\xi \xi f_a \text{ with } \xi = \frac{v_\parallel}{v}$$

Then in order to take into account momentum exchange between species while keeping the total momentum constant, a second velocity $U_{\parallel ab}$ is chosen as

$$U_{\parallel ab} = \frac{\left\langle \nu_{s,ab} v^2 U_{\parallel d,a}\right\rangle_a}{\left\langle \nu_{s,ab} v^2\right\rangle_a}$$

A dimensionless parameter q_{ab} accounting for energy exchange between species is defined as

$$q_{ab} = T_b \frac{\left\langle \nu_{E,ab}\frac{m_a v^2}{2} f_a\right\rangle_a}{\left\langle \nu_{E,ab}\left(\frac{m_a v^2}{2}\right)^2\right\rangle_a}$$

The bracket corresponds to mean values in velocity space $< ... >= \int d^3\boldsymbol{v}\frac{F_{M0a}}{n_a}...$. Different frequencies appear in the previous expressions. They are defined as follow :

- the Hirshman and Sigmar's inter-species collision frequency [12]

$$\nu^{HS}_{ab} = \sqrt{2}\frac{N_b Z_b^2}{N_a Z_a^2}\nu_{aa}$$

- the velocity modulus diffusion rate

$$\nu_{v,ab}(x_a) = \nu^{HS}_{ab} x_{ba}\frac{\Theta(x_b)}{x_a^2}$$

- the deflection frequency

$$\nu_{d,ab}(x_a) = \nu^{HS}_{ab} x_{ba}\frac{\Psi(x_b)}{x_a^2}$$

- the slowing-down frequency

$$\nu_{s,ab} = \nu^{HS}_{ab}\left(1 + \frac{m_a}{m_b}\right) x_{ba}^3 \Theta(x_b)$$

- the energy-loss rate is defined as

$$\nu_{E,ab} = -\frac{1}{v^4 F_{M0a}}\frac{\partial}{\partial v}\left(\nu_{v,ab} F_{M0a} v^5\right)$$

Where the ratio between the thermal velocities is introduced $x_{ba} = \frac{v_{Ta}}{v_{Tb}}$. We also define the following functions

$$\Psi(x) = \frac{3\sqrt{\pi}}{4}\frac{1}{x}\left[\Phi(x) - G(x)\right]$$

$$\Theta(x) = \frac{3\sqrt{\pi}}{2}\frac{G(x)}{x}$$

$$G(x) = \frac{1}{2x^2}\left[\Phi(x) - x\Phi'(x)\right]$$

$$\Phi(x) = \frac{2}{\sqrt{\pi}}\int_0^x dy \exp\left(-y^2\right)$$

The function Φ is the error function and G is the Chandrasekhar function. The different frequencies normalized to ν^{HS}_{ab} are plotted in figure (1)

Figure 1: Velocity dependance of the different frequencies

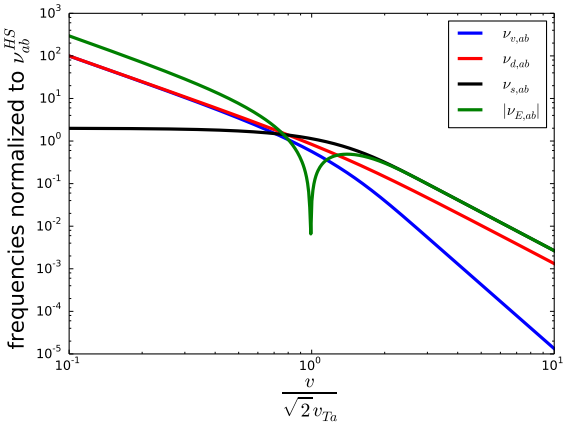

3. Numerical implementation of the collision operator

3.1. Separation of the different collision terms

The collision operator is difficult to treat as a whole. It is much easier to split the different parts of the operator and treat them separately with a time splitting scheme. The first step is to discriminate the evolutions of F_{M0a} and δF_a via collisions. The equation that needs to be solved is

$$\frac{\partial F_a}{\partial t} = \sum_b C_{ab}\left(F_a, F_b\right)$$

which can be split as

$$\begin{cases} \frac{\partial F_{M0a}}{\partial t} = \sum_b C^0_{ab}\left(F_{M0a}, F_{M0b}\right) \\ \frac{\partial \delta F_a}{\partial t} = \sum_b C^1_{ab}\left(F_a, F_b\right) \end{cases}$$

The second equation of the system can be recast as the evolution of the total distribution assuming that the Maxwellian is unchanged. This alternative expression is valid as the evolution of the Maxwellian is treated by the first equation. This new expression is useful especially for the treatment of the μ derivatives.

$$\frac{\partial F_a}{\partial t} = \sum_b C^1_{ab}\left(F_a, F_b\right) \text{ with } F_{M0a} = cst$$

A second step is to separate the evolution of δF_a in two parts. Indeed, the evolution governed by $C_{v,ab} + C_{d,ab}$ is difficult to treat as it includes μ derivatives. It will be treated differently from $C_{\parallel,ab}$ which is easier to implement. In the end, the problem can be split in three parts : the evolution of the Maxwellian due to C^0_{ab}, the evolution of the distribution function due to $C_{\parallel,ab}$, and the evolution of the distribution function due to $C_{v,ab} + C_{d,ab}$. The last two steps are performed by assuming that the Maxwellian F_{M0a} remains constant.

$$\begin{cases} \frac{\partial F_{M0a}}{\partial t} = \sum_b C^0_{ab}\left(F_{M0a}, F_{M0b}\right) & \\ \frac{\partial F_a}{\partial t} = \sum_b C_{\parallel,ab}\left(F_a, F_b\right) & \left(F_{M0a} = cst\right) \\ \frac{\partial F_a}{\partial t} = \sum_b C_{v,ab}\left(F_a, F_b\right) + C_{d,ab}\left(F_a, F_b\right) & \left(F_{M0a} = cst\right) \end{cases} \tag{1}$$

3.2. Evolution of thermal energy

Here we detail how the thermal energy evolves due to collisions. The effect of C^0_{ab} is to exchange thermal energy between Maxwellians. The thermal energy exchange is exactly known in the case of Maxwellians. It is made of two contributions : the first term corresponds to the thermal energy equirepartition and the second one corresponds to the opposite of the work of the friction force.

$$Q_{M,ab} = -3n_a\frac{m_a}{m_a+m_b}\nu_{ab}\left(T_a - T_b\right) + n_a m_a \nu_{ab} V_{\parallel a}\left(V_{\parallel a} - V_{\parallel b}\right)$$

The evolution of thermal energy is governed by $Q_{M,ab}$

$$\frac{3}{2}n_a\frac{\partial T_a}{\partial t} = \sum_b Q_{M,ab}$$

which is equivalent to

$$\frac{\partial T_a}{\partial t} = \sum_b m_a \nu_{ab}\left[\frac{2}{m_a+m_b}\left(T_b - T_a\right) + \frac{2}{3}V_{\parallel a}\left(V_{\parallel a} - V_{\parallel b}\right)\right] \tag{2}$$

This relation will be used to compute the evolution of the Maxwellian distribution in eq.(1). Notice that the total (thermal + kinetic) energy remains unaffected by the latter term, as it should to preserve Galilean invariance.

3.3. Approximation of the distribution function

The quantities $U_{\parallel ab}$ and q_{ab} are difficult to compute numerically . Indeed both include collision frequencies ($\nu_{s,ab}$ and $\nu_{E,ab}$) that depend on the mass ratio $\frac{m_a}{m_b}$ and the integrals are then difficult to compute in the two limits $\frac{m_a}{m_b} \gg 1$ and $\frac{m_a}{m_b} \ll 1$. An analytical approach is used to overcome this difficulty.

3.3.1. Development on a set of orthogonal polynomials

Following the method developped by Hirshman and Sigmar [13], the distribution function is projected on a set of orthogonal polynomials

$$F(v,\theta,\varphi_c) = \sum_{\ell,m} F_{\ell,m}(v) Y_{\ell,m}(\theta,\varphi_c)$$

with φ_c the phase of the cyclotronic motion and $Y_{\ell,m}(\theta,\varphi_c)$ the spherical harmonics

$$Y_{\ell,m}(\theta,\varphi_c) = P_{\ell,m}(\xi)e^{im\varphi_c} \text{ and } \cos\theta = \xi = \frac{v_\parallel}{v}$$

As the method is used in a gyrokinetic approach only the $m = 0$ component is kept :

$$F(v,\theta) = \sum_\ell F_\ell(v) P_\ell(\xi)$$

where P_ℓ are Legendre polynomials.

Then each component $F_\ell(v)$ is expanded in Laguerre polynomials

$$F_\ell(v) = \sum_j \left(\frac{v}{2v^2_{Ta}}\right)^\ell \mathcal{F}^{(\ell)}_j L^{(\ell+\frac{1}{2})}_j(x^2_a) F_{M0a}$$

with

$$\mathcal{F}^{(\ell)}_j = \left\langle F_\ell | L^{(\ell+\frac{1}{2})}_j \right\rangle = \frac{2\pi^{3/2} j!}{\Gamma(j+\ell+\frac{3}{2})}\int_0^\infty v^\ell L^{(\ell+\frac{1}{2})}_j(x^2_a)\frac{F_\ell(v)}{n_a}v^2 dv$$

where $L^{(\ell+\frac{1}{2})}_j$ is the generalized Laguerre polynomial of order $\ell+\frac{1}{2}$. Notice that the $L^{(\ell+\frac{1}{2})}_j$ are chosen as functions of v^2. The underlying will is that the lowest order terms of the development capture explicitely the two motion invariants $E\&P_\varphi$, which are relevant at low collisionality. Indeed, $(l=1, j=0)$ scales like $v_\parallel$, hence capturing the P_φ, while $(l=0, j=1)$ scales like v^2 which corresponds to the energy. Using these defintions it is possible to show that

$$\mathcal{F}^{(0)}_0 = 1$$

$$\mathcal{F}^{(0)}_1 = 0$$

$$\mathcal{F}^{(0)}_2 = \frac{2}{15}\left(\left\langle x^4_a f_a\right\rangle_a - \frac{15}{4}\right) = \frac{2}{15}\left\langle x^4_a\left(f_a - 1\right)\right\rangle$$

where $f_a = \frac{F_a}{F_{M0a}}$ is the normalized distribution function

$$\mathcal{F}_0^{(1)} = 2V_{\parallel a}$$

and

$$\mathcal{F}_1^{(1)} = -\frac{4q_{\parallel a}}{5n_aT_a} = -\frac{4}{5}\left\langle v_\parallel\left(x_a^2 - \frac{5}{2}\right)f_a\right\rangle_a \tag{3}$$

Then keeping only the first two polynomials in both direction, the normalized distribution function can be approximated by

$$f_a \simeq 1 + \frac{v_\parallel}{v_{Ta}^2}\left[V_{\parallel a} - \frac{q_{\parallel a}}{n_aT_a}\left(1 - \frac{2x_a^2}{5}\right)\right] \tag{4}$$

3.3.2. Expression of $C_{\parallel,ab}$

The $C_{\parallel,ab}$ term deals with momentum exchange between different species. Indeed one can show that the rate of momentum exchange of the total operator is given by

$$R_{\parallel ab} = -n_am_a\nu_{ab}\left(U_{\parallel ab} - U_{\parallel ba}\right)$$

To evaluate the two quantities $U_{\parallel d,a}(v)$ and $U_{\parallel ab}$ the approximate distribution function (4) is used. It gives :

$$U_{\parallel d,a} = V_{\parallel a} - \frac{q_{\parallel a}}{n_aT_a}\left(1 - \frac{2}{5}x_a^2\right) \tag{5}$$

$$U_{\parallel ba} = V_{\parallel b} - \frac{3}{5}\frac{q_{\parallel b}}{n_bT_b}\left(\frac{1}{1+x_{ba}^2}\right)$$

and so

$$\begin{aligned} C_{\parallel,ab} &= \nu_{s,ab}\frac{m_a}{T_a}v_\parallel F_{M0a} \\ &\times \left[V_{\parallel b} - V_{\parallel a} + \frac{q_{\parallel a}}{n_aT_a}\left(1 - \frac{2}{5}x_a^2\right) - \frac{3}{5}\frac{q_{\parallel b}}{n_bT_b}\left(\frac{1}{1+x_{ba}^2}\right)\right] \end{aligned}$$

The collisional drag force becomes

$$\begin{aligned} R_{\parallel ab} &= -n_am_a\nu_{ab} \\ &\times \left[V_{\parallel a} - V_{\parallel b} - \frac{3}{5}\frac{q_{\parallel a}}{n_aT_a}\left(\frac{1}{1+x_{ab}^2}\right) + \frac{3}{5}\frac{q_{\parallel b}}{n_bT_b}\left(\frac{1}{1+x_{ba}^2}\right)\right] \end{aligned} \tag{6}$$

For a Maxwellian, the result is exact and reduces to the friction force :

$$R_{\parallel M,ab} = -n_am_a\nu_{ab}\left[V_{\parallel a} - V_{\parallel b}\right]$$

To ensure this property, one needs $q_{\parallel a} = 0$ for a Maxwellian distribution function. Then the definition of $q_{\parallel a}$ is changed accordingly :

$$q_{\parallel a} = \frac{1}{2}\int d^3\boldsymbol{v}m_a\left[\left(v_\parallel - V_{\parallel a}\right)^2 + v_\perp^2\right]\left(v_\parallel - V_{\parallel a}\right)F_a$$

This new defintion is equivalent to the one used in eq.(3) in the limit of small Mach number. It is the one used in [7].

A long but straightforward calculation allows one to show that for the simplified distribution function (4) $q_{ab} = 0$. This approximation will be used in the rest of this article. Then g_{ab} becomes $g_a = f_a - \frac{m_av_\parallel U_{\parallel d,a}}{T_a}$.

3.4. Treatement of the μ derivatives

Derivatives with respect to μ are present in the terms $C_{v,ab}$ and $C_{d,ab}$. The treatment of these derivatives by finite differences may be problematic if one wants to use a relatively low resolution in the μ direction. An alternative method based on a projection on orthogonal polynomials in μ is adopted. It allows one to solve the problem while keeping a relatively low resolution in the μ direction (typically $N_\mu = 64$). The equation solved with this method is

$$\frac{\partial F_a}{\partial t} = \sum_b C_{v,ab}(F_a, F_b) + C_{d,ab}(F_a, F_b) \Leftrightarrow \frac{\partial f_a}{\partial t} = \sum_b \bar{C}_{ab} \tag{7}$$

where we have defined the normalized collision operator $\bar{C}_{ab}(F) = \frac{C_{v,ab}(F)+C_{d,ab}(F)}{F_{M0a}}$. This approach is possible because a Maxwellian is in the kernel of $C_{v,ab} + C_{d,ab}$. This term can be expressed differently to simplify its numerical treatment.

$$\begin{aligned} \bar{C}_{ab}(g_a) &= K_{1,ab}\frac{\partial g_a}{\partial v_\parallel} + K_{2,ab}\frac{\partial^2 g_a}{\partial v_\parallel^2} + K_{3,ab}u\frac{\partial^2 g_a}{\partial v_\parallel \partial u} \\ &\quad + K_{4,ab}u\frac{\partial g_a}{\partial u} + \bar{C}_{m,ab}(g_a) \end{aligned}$$

where $u = \frac{\mu B}{T_a}$. Defining $D_{d,ab} = \frac{1}{2}\nu_{d,ab}v^2$ and setting $B_\parallel^\star = B$, it is possible to show that

$$\begin{aligned} K_{1,ab} &= v_\parallel\left[\frac{1}{v}\frac{\partial D_{d,ab}}{\partial v} - \frac{D_{d,ab}}{v_{Ta}^2}\right] + v_\parallel\left(\nu_{v,ab} - \nu_{d,ab}\right)\left(2 - x_a^2\right) \\ &+ \frac{v_\parallel v}{2}\frac{\partial\left(\nu_{v,ab} - \nu_{d,ab}\right)}{\partial v} \end{aligned}$$

$$K_{2,ab} = D_{d,ab} + \frac{v_\parallel^2}{2}\left(\nu_{v,ab} - \nu_{d,ab}\right)$$

$$K_{3,ab} = 2v_\parallel\left(\nu_{v,ab} - \nu_{d,ab}\right)$$

$$K_{4,ab} = \left(1 - \frac{v_\parallel^2}{v_{Ta}^2}\right)\left(\nu_{v,ab} - \nu_{d,ab}\right) + \frac{v_\parallel^2}{v}\frac{\partial\left(\nu_{v,ab} - \nu_{d,ab}\right)}{\partial v}$$

$$\bar{C}_{m,ab}(g_a) = \frac{2}{v_{Ta}^2F_{M0a}}\frac{\partial}{\partial u}\left[F_{M0a}\left(D_{d,ab} + v_{Ta}^2u\left(\nu_{v,ab} - \nu_{d,ab}\right)\right)u\frac{\partial g_a}{\partial u}\right]$$

f is projected on a set of orthogonal polynomials:

$$f_a(\boldsymbol{r}, v_\parallel, u, t) = \sum_l \alpha_{\ell,a}(\boldsymbol{r}, v_\parallel, t)P_\ell(u)$$

Projecting equation (7) on polynomial P_ℓ gives

$$\frac{\partial \alpha_{\ell,a}}{\partial t} = \sum_b \left\langle \bar{C}_{ab}(g_a)\,|P_\ell\right\rangle$$

In practice, Laguerre polynomials are chosen. Thus it defines the scalar product as

$$\langle f|g\rangle = \int_0^\infty dx f(x)\,g(x)$$

3.5. Evolution equation of the distribution function components

3.5.1. Projection of g_a on Laguerre polynomials

The first step is to compute the projection of g_a on Laguerre polynomials. The same approximation as the one used in the computation of $C_{\parallel,ab}$ is considered (eq.5). In that case

$$\begin{aligned} g_a &= f_a - \frac{m_a v_\parallel U_{\parallel d,a}}{T_a} \\ &= f_a + P_0(u)\kappa_{0,a} + P_1(u)\kappa_{1,a} \end{aligned}$$

with

$$\kappa_{0,a} = -\left\{ \frac{m_a v_\parallel}{T_a} \left[V_{\parallel a} - \frac{q_{\parallel a}}{n_a T_a} \left(\frac{3}{5} - \frac{m_a v_\parallel^2}{5T_a} \right) \right] \right\}$$

and

$$\kappa_{1,a} = \frac{2 m_a v_\parallel q_{\parallel a}}{5 n_a T_a^2}$$

So g_a can be easily projected on Laguerre polynomials

$$g_a = \sum_i \alpha_{i,a}^{'} P_i$$

with

$$\begin{cases} \alpha'_{i,a} = \alpha_{i,a} + \kappa_{i,a} & \text{if } i < 2 \\ \alpha'_{i,a} = \alpha_{i,a} & \text{otherwise} \end{cases}$$

3.5.2. Expression of the $C_v + C_d$ part of the operator

Using the properties of Laguerre polynomials, and summing over the species, eq.(7) can be written

$$\frac{\partial \alpha_{\ell,a}}{\partial t} = \sum_j \left[\alpha_{j,a}^{'} N_{0,a}^{jl} + \frac{\partial \alpha_{j,a}^{'}}{\partial v_\parallel} N_{1,a}^{jl} + \frac{\partial^2 \alpha_{j,a}^{'}}{\partial v_\parallel^2} N_{2,a}^{jl} \right] \quad (8)$$

with

$$N_{0,a}^{jl} = \sum_b \left\langle j K_{4,ab} \left(P_j - P_{j-1} \right) + \bar{C}_{m,ab}(P_j) | P_l \right\rangle$$

$$N_{1,a}^{jl} = \sum_b \left\langle K_{1,ab} P_j + j K_{3,ab} \left(P_j - P_{j-1} \right) | P_l \right\rangle$$

$$N_{2,a}^{jl} = \sum_b \left\langle K_{2,ab} P_j | P_l \right\rangle$$

At this stage, these quantities remain somewhat too intricate to be computed analytically. Using the definitions given in the previous part and defining the following quantities

$$P_j P_\ell = \sum_{i=0}^{j+\ell} C_{j\ell}^i u^i$$

$$L_{i,ab}^{(0)} = \left\langle \frac{D_{d,ab}}{v_{Ta}^2} | u^i \right\rangle$$

$$L_{i,ab}^{(1)} = \left\langle \frac{1}{v} \frac{\partial D_{d,ab}}{\partial v} | u^i \right\rangle$$

$$L_{i,ab}^{(2)} = \left\langle \nu_{v,ab} - \nu_{d,ab} | u^i \right\rangle$$

$$L_{i,ab}^{(3)} = \left\langle \frac{v}{2} \frac{\partial \left(\nu_{v,ab} - \nu_{d,ab} \right)}{\partial v} | u^i \right\rangle$$

$$L_{i,ab}^{(4)} = \left\langle \frac{v_{Ta}^2}{v} \frac{\partial \left(\nu_{v,ab} - \nu_{d,ab} \right)}{\partial v} | u^i \right\rangle$$

it can be shown that

$$\begin{aligned} N_{0,a}^{jl} &= j \sum_b \sum_{i=0}^{j+\ell} C_{j\ell}^i \begin{bmatrix} -2L_{i,ab}^{(0)} + 2L_{i,ab}^{(1)} + \left(3 - \frac{v_\parallel^2}{v_{Ta}^2} \right) L_{i,ab}^{(2)} \\ -2L_{i+1,ab}^{(2)} + \left(2 + \frac{v_\parallel^2}{v_{Ta}^2} \right) L_{i,ab}^{(4)} \end{bmatrix} \\ &- j \sum_b \sum_{i'=0}^{j+\ell-1} C_{j-1,\ell}^{i'} \begin{bmatrix} 2L_{i',ab}^{(1)} + \left(3 - \frac{v_\parallel^2}{v_{Ta}^2} \right) L_{i',ab}^{(2)} \\ + \left(2 + \frac{v_\parallel^2}{v_{Ta}^2} \right) L_{i',ab}^{(4)} \end{bmatrix} \end{aligned}$$

$$\begin{aligned} N_{1,a}^{jl} &= v_\parallel \sum_b \sum_{i=0}^{j+\ell} C_{j\ell}^i \begin{bmatrix} -L_{i,ab}^{(0)} + L_{i,ab}^{(1)} + \left(2 + 2j - \frac{v_\parallel^2}{2v_{Ta}^2} \right) L_{i,ab}^{(2)} \\ -L_{i+1,ab}^{(2)} + L_{i,ab}^{(3)} \end{bmatrix} \\ &- v_\parallel \sum_b \sum_{i'=0}^{j+\ell-1} C_{j-1,\ell}^{i'} 2j L_{i',ab}^{(2)} \end{aligned}$$

$$N_{2,a}^{jl} = \sum_b \sum_{i=0}^{j+\ell} C_{j\ell}^i v_{Ta}^2 \left[L_{i,ab}^{(0)} + \frac{v_\parallel^2}{2v_{Ta}^2} L_{i,ab}^{(2)} \right]$$

3.5.3. Computation of the scalar products

Integrating by parts, it is possible to show that

$$\begin{cases} L_{0,ab}^{(1)} = & -\frac{D_{d,ab}\left(v_\parallel, u=0\right)}{v_{Ta}^2} + L_{0,ab}^{(0)} \\ L_{i,ab}^{(1)} = & L_{i,ab}^{(0)} - i L_{i-1,ab}^{(0)} \text{ for } i > 0 \end{cases}$$

$$\begin{cases} L_{0,ab}^{(3)} = & \frac{v_\parallel^2}{2v_{Ta}^2} \left[L_{0,ab}^{(2)} - \left(\nu_{v,ab} - \nu_{d,ab} \right) \left(v_\parallel, u = 0 \right) \right] + L_{1,ab}^{(2)} - L_{0,ab}^{(2)} \\ L_{i,ab}^{(3)} = & \frac{v_\parallel^2}{2v_{Ta}^2} \left[L_{i,ab}^{(2)} - i L_{i-1,ab}^{(2)} \right] + L_{i+1,ab}^{(2)} - (i+1) L_{i,ab}^{(2)} \text{ for } i > 0 \end{cases}$$

$$\begin{cases} L_{0,ab}^{(4)} = & L_{0,ab}^{(2)} - \left(\nu_{v,ab} - \nu_{d,ab} \right) \left(v_\parallel, u = 0 \right) \\ L_{i,ab}^{(3)} = & L_{i,ab}^{(2)} - i L_{i-1,ab}^{(2)} \text{ for } i > 0 \end{cases}$$

The only last difficulty is then to compute $L_{i,ab}^{(0)}$ and $L_{i,ab}^{(2)}$. Unfortunately, the v dependences of $\nu_{v,ab}$ and $\nu_{d,ab}$ prevent one to compute these scalar products analytically without approximation. On the other hand a numerical approach would be too costly. A solution consists in fitting the v dependence of $D_{d,ab}$ and $(\nu_{v,ab} - \nu_{d,ab})$ by suitable functions that enable an analytic computation of the scalar products. The following fits are made

$$\begin{cases} \frac{D_{d,ab}}{v_{Ta}^2} & = \frac{0.75\sqrt{\pi}}{\sqrt{x_a^2 + \frac{9\pi}{16}\left(\frac{v_{Ta}}{v_{Tb}} \right)^2}} \nu_{ab}^{HS} \\ \nu_{v,ab}\text{-}\nu_{d,ab} & = -\frac{0.75\sqrt{\pi}}{\left(x_a^2 + 2.1 \left(\frac{v_{Ta}}{v_{Tb}} \right)^2 \right)^{3/2}} \nu_{ab}^{HS} \end{cases}$$

The fits are given respectively in figures 2 and 3 for the self collision case which is the most sensitive one.

Figure 2: Fitting for $D_{d,ab}$

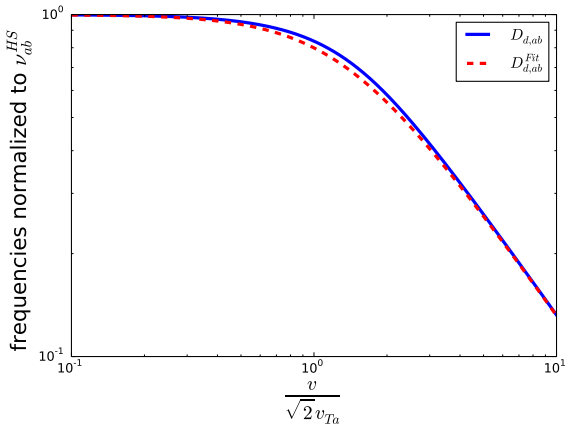

Figure 3: Fitting for $\nu_{v,ab} - \nu_{d,ab}$

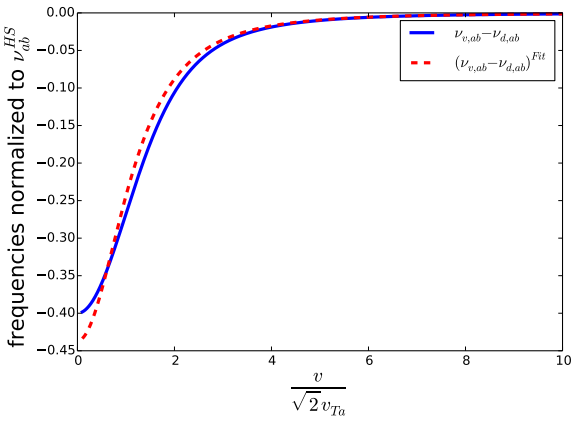

Thanks to these fits, the scalar products can be approximated by analytical expressions :

$$L_{i,ab}^{(0)} = 0.75\sqrt{\pi}\nu_{ab}^{HS} I_i^{(0)} \left(\frac{v_\parallel^2}{2v_{Ta}^2} + \frac{9\pi}{16}\frac{v_{Tb}^2}{v_{Ta}^2} \right)$$

$$L_{i,ab}^{(2)} = -0.75\sqrt{\pi}\nu_{ab}^{HS} I_i^{(1)} \left(\frac{v_\parallel^2}{2v_{Ta}^2} + 2.1\frac{v_{Tb}^2}{v_{Ta}^2} \right)$$

With

$$I_i^{(n)}(x) = \int_0^\infty du \frac{u^i e^{-u}}{(u+x)^{n+1/2}}$$

It can be shown that

$$I_i^{(n)}(x) = e^x \sum_{k=0}^{i} \begin{pmatrix} i \\ k \end{pmatrix} (-x)^{i-k} J_{k-n}(x)$$

where

$$J_i(x) = \int_x^\infty du\ e^{-u} u^{i-1/2}$$

which can be easily computed by recurrence.

3.6. Numerical implementation

3.6.1. Numerical schemes

An explicit scheme is used to compute the evolution of the distribution function due to C_{ab}^0 and $C_{\parallel ab}$. Eq.(8) is solved with a Crank-Nicholson scheme [5] for stability reasons. The resolution of the Crank-Nicholson is detailed here : the problem can be written in a vectorized form

$$\frac{\partial \boldsymbol{\alpha}}{\partial \hat{t}} = T\boldsymbol{\alpha} + \boldsymbol{S}$$

with

$$\boldsymbol{\alpha} = \begin{pmatrix} \vdots \\ \alpha_0^{(k)} \\ \alpha_1^{(k)} \\ \vdots \\ \alpha_{Npol-1}^{(k)} \\ \alpha_0^{(k+1)} \\ \vdots \end{pmatrix}$$

and $0 \leq k \leq k_{max}$,

$$T = \begin{pmatrix} B_0 & C_0 & 0 & 0 & 0 & 0 & 0 \\ A_1 & B_1 & C_1 & 0 & 0 & 0 & 0 \\ 0 & A_2 & B_2 & C_2 & 0 & 0 & 0 \\ 0 & 0 & . & . & . & 0 & 0 \\ 0 & 0 & 0 & . & . & . & 0 \\ 0 & 0 & 0 & 0 & . & . & C_{k_{max}-1} \\ 0 & 0 & 0 & 0 & 0 & A_{k_{max}} & B_{k_{max}} \end{pmatrix}$$

where N_{pol} is the number of Laguerre polynomials that are kept, k is the index associated with the $v_\parallel$ direction, and the A_k, B_k, C_k are square blocks of size N_{pol}. Their respective components are

$$\begin{cases} a_{lj}^{(k)} = & -\frac{\hat{N}_{1,a}^{jl(k)}}{2\Delta v_\parallel} + \frac{\hat{N}_{2,a}^{jl(k)}}{\Delta v_\parallel^2} \\ b_{lj}^{(k)} = & \hat{N}_{0,a}^{jl(k)} - 2\frac{\hat{N}_{2,a}^{jl(k)}}{\Delta v_\parallel^2} \\ c_{lj}^{(k)} = & \frac{\hat{N}_{1,a}^{jl(k)}}{2\Delta v_\parallel} + \frac{\hat{N}_{2,a}^{jl(k)}}{\Delta v_\parallel^2} \end{cases}$$

and

$$\boldsymbol{S} = \begin{pmatrix} \vdots \\ S_0^{(k)} = \kappa_{0,a}^{(k)}\hat{N}_{0,a}^{jl} + \frac{\partial \kappa_{0,a}^{(k)}}{\partial \hat{v}_\parallel}\hat{N}_{1,a}^{jl} + \frac{\partial^2 \kappa_{0,a}^{(k)}}{\partial \hat{v}_\parallel^2}\hat{N}_{2,a}^{jl} \\ S_1^{(k)} = \kappa_{1,a}^{(k)}\hat{N}_{1,a}^{jl} + \frac{\partial \kappa_{1,a}^{(k)}}{\partial \hat{v}_\parallel}\hat{N}_{1,a}^{jl} + \frac{\partial^2 \kappa_{1,a}^{(k)}}{\partial \hat{v}_\parallel^2}\hat{N}_{2,a}^{jl} \\ S_2^{(k)} = 0 \\ \vdots \\ S_{Npol-1}^{(k)} = 0 \\ \vdots \end{pmatrix}$$

The Cranck Nicholson scheme is split in the following way

$$\begin{cases} \left(I - \frac{\Delta t}{4}T^n\right)\tilde{\boldsymbol{\alpha}} & = \left(I + \frac{\Delta t}{4}T^n\right)\boldsymbol{\alpha}^n \\ \tilde{\tilde{\boldsymbol{\alpha}}} & = \tilde{\boldsymbol{\alpha}} + \Delta t \boldsymbol{S}^n \\ \left(I - \frac{\Delta t}{4}T^n\right)\boldsymbol{\alpha}^{n+1} & = \left(I + \frac{\Delta t}{4}T^n\right)\tilde{\tilde{\boldsymbol{\alpha}}} \end{cases}$$

where n stands for the time index and I is the identity matrix. The scheme is split for stability reason. Indeed, the tridiagonal by blocks inversion problem can be solved thanks to a LU decomposition valid only if the left hand side matrix is diagonal dominant. This condition gives a limit on the time step for collision as the dominant off diagonal term is proportionnal to $\frac{\Delta t}{\Delta v_\parallel^2}$. Interestingly the splitting allows for a time step twice bigger than the one without splitting.

3.6.2. Numerical implementation of conservation properties

Due to numerical approximations, conservation properties are not perfectly satisfied. We present here a method used to improve these conservation laws. It is used to correct only the C^1 part. Indeed the way C^0 is treated automatically satisfies conservation properties. All fluid quantities without indices correspond to the initial values. The ones noted with the prime correspond to values after the use of C^1. Finally the quantities with two primes are corrected values. The procedure is the following, in chronological order :

i)we correct the density by simply applying an homothety on the distribution function

$$F'' = \frac{F'n}{n'}$$

ii) the parallel velocity and the temperature are then corrected simultanously by removing the Maxwellian after collisions F'_M and adding a new Maxwellian F''_M with the corrected moments defined as

$$\begin{cases} V''_{\|a} = & V_{\|a} + \Delta t \sum_b \frac{R_{\|ab}}{n_a m_a} \\ T''_a = & T_a \end{cases}$$

The corrected parallel velocity comes from the momentum evolution equation

$$n_a m_a \frac{\partial V_{\|a}}{\partial t} = \sum_b R_{\|ab}$$

where the exchange rate of momentum is given by (6). The temperature has to be kept constant $T'' = T$ to be consistent with the development made in section 3.3.2. Indeed, one can show that the exchange rate of energy due to C^1_{ab} is :

$$W^1_{ab} = W_{\|ab} + W_{v,ab} + W_{d,ab}$$

with $W_{\|ab}$ the work of the drag force

$$W_{\|ab} = V_{\|a} R_{\|ab}$$

and

$$W_{v,ab} + W_{d,ab} = \frac{3T_a T_b n_a m_a \nu_{ab}}{m_a + m_b} \left(\frac{q_{ba}}{T_a} - \frac{q_{ab}}{T_b} \right) = 0 \text{ as } q_{ab} = 0$$

It follows that the energy evolution of species a due to the C^1 part is then given by

$$\frac{3}{2} n_a \left. \frac{\partial T_a}{\partial t} \right|_{C^1} + n_a m_a V_{\|a} \frac{\partial V_{\|a}}{\partial t} = \sum_b W^1_{ab} \Rightarrow \left. \frac{\partial T_a}{\partial t} \right|_{C^1} = 0$$

4. Validation of the collision operator

4.1. Tests of the collision operator alone

To validate the collision operator, a first step is to make conservation and relaxation tests by solving collisions only, i.e. without the effects of trajectories

$$\frac{\partial f_a}{\partial t} = \sum_b C_{ab}$$

In this section critical physical properties of the collision operator are tested : conservation properties, relaxation toward the Maxwellian and its dynamics and the exchange rates of momentum and energy between species. All the results shown here are obtained with a discretization of $(N_{v_\|}, N_\mu) = (128, 64)$ which is the optimal discretization for this operator. For these simulations, the collisionality of the main species is $\nu_\star = 1$. For the single species cases, the time step in GYSELA is $\Delta t = 100\omega_{ci}$. For the multispecies cases performed with deuterium as first species and tungsten as second species, the time step is reduced to take into account that the collisionality of the impurity is higher than the one of the main species. These tests are performed without gyroaverage to be consistent with the fact that FLR effects are not included in the present version of the collision operator.

4.1.1. Single species tests

Conservation laws are tested by initializing a Maxwellian that belongs to the kernel of the operator and should therefore remain constant in time. After approximately one collision time, the following conservation are observed for an initial mach number $M_\| = 0$:

$$\frac{\Delta n}{n} \simeq 7 \cdot 10^{-7} \qquad \Delta p_\| \simeq 10^{-9} \qquad \frac{\Delta E}{E} \simeq 6 \cdot 10^{-6}$$

For an initial Mach number of $M_\| = 1$ comparable conservation properties are found. This means than the collision operator can be used for Mach numbers $M_\| \leq 1$ without any breakdown of its conservation properties.

Relaxation toward the Maxwellian has been tested by initialazing two different distribution functions. For the parallel direction, the initial distribution function is chosen as

$$F_a = F_{M0a} \left(1 + \frac{m_a v_\|^2}{2T_a} \right)$$

For the perpendicular direction, the initial distribution function is

$$F_a = F_{M0a} \left(1 + \frac{m_a v_\perp^2}{2T_a} \right)$$

The results are shown on figure (4) . As expected a relaxation toward the Maxwellian is observed in both cases after a few collision times.

Figure 4: Relaxation in velocity space

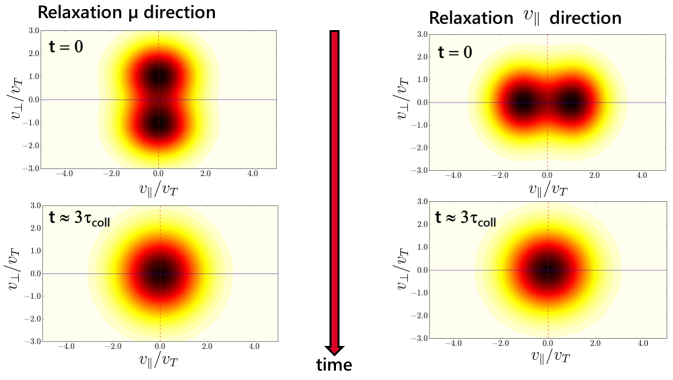

To investigate the dynamical relaxation to the Maxwellian,

a case with $T_\parallel \neq T_\perp$ and $\frac{T_\parallel - T_\perp}{T_a} \ll 1$ is launched

$$F_a = n_a \left(\frac{m_a}{2\pi T_{\parallel a}}\right)^{1/2} \frac{m_a}{2\pi T_{\perp a}} \exp\left(-\frac{m_a v_\parallel^2}{2T_{\parallel a}} - \frac{m_a v_\perp^2}{2T_{\perp a}}\right)$$

where $T_a = \frac{T_{\parallel a} + 2T_{\perp a}}{3}$. Then at first order in $\frac{T_\parallel - T_\perp}{T_a} \ll 1$

$$f_a = 1 + \frac{T_{\parallel a} - T_{\perp a}}{3T_a} \frac{1}{v_{Ta}^2}\left(v_\parallel^2 - \frac{v_\perp^2}{2}\right)$$

Integrating $\partial_t f_a$, weighted by the energy, over the velocity space leads to :

$$\frac{d\ln\left(T_\parallel - T_\perp\right)}{dt} = \frac{16}{15\sqrt{\pi}} \int_0^\infty dx e^{-x^2} x^6 \left(\nu_v + \frac{3}{2}\nu_d\right)$$

This integral can be computed either with the actual expressions of ν_v and ν_d or their approximate values :

$$\begin{cases} \frac{d\ln\left(T_\parallel - T_\perp\right)}{dt} & = -0.80\nu_{aa} \text{ for actual expressions} \\ \frac{d\ln\left(T_\parallel - T_\perp\right)}{dt} & = -0.78\nu_{aa} \text{ for fitted values} \end{cases}$$

The discrepancy is small, thus validating the relevance of the fitting represented in figures (2) and (3). The prediction for the actual expressions of ν_v and ν_d is used as a theoretical prediction and compared with GYSELA results in figure (5). A mismatch of 15% percent is found. This discrepancy is acceptable as most of physics phenomena studied with gyrokinetic codes are independent of the isotropisation rate.

Figure 5: Time evolution of $T_\parallel$ and $T_\perp$

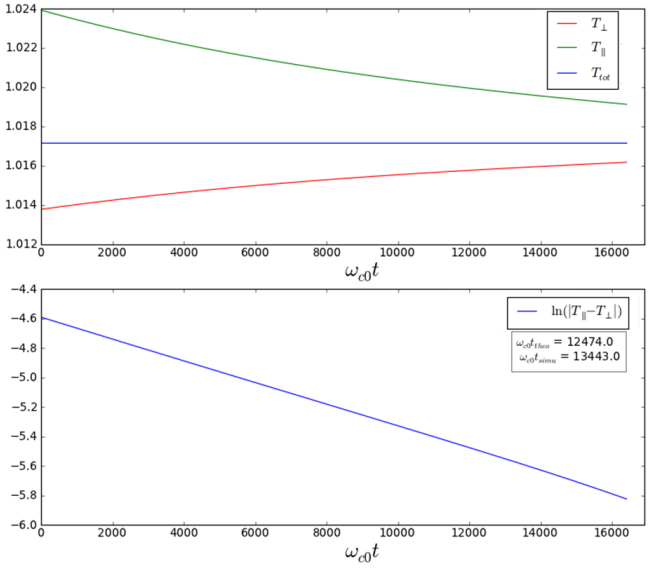

4.1.2. Test with two species

The exchange rates of parallel momentum and energy between two Maxwellians are respectively

$$R_{\parallel,Mab} = -n_a m_a \nu_{ab}\left(V_{\parallel a} - V_{\parallel b}\right)$$

$$Q_{M,ab} = -3\frac{n_a m_a}{m_a + m_b}\nu_{ab}\left(T_a - T_b\right)$$

It is then easy to show that

$$\frac{d\ln\left(V_{\parallel a} - V_{\parallel b}\right)}{dt} = -\left(\nu_{ab} + \nu_{ba}\right)$$

$$\frac{d\ln\left(T_a - T_b\right)}{dt} = -2\frac{m_a\nu_{ab} + m_b\nu_{ba}}{m_a + m_b}$$

These two relations have been checked. The results for the velocities are shown in fig.6 and for temperature in fig.7. The agreement is within one percent.

Figure 6: Relaxation $V_\parallel$ two species

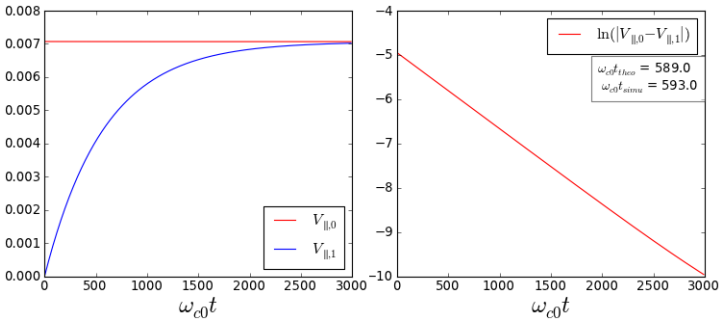

Figure 7: Relaxation T two species

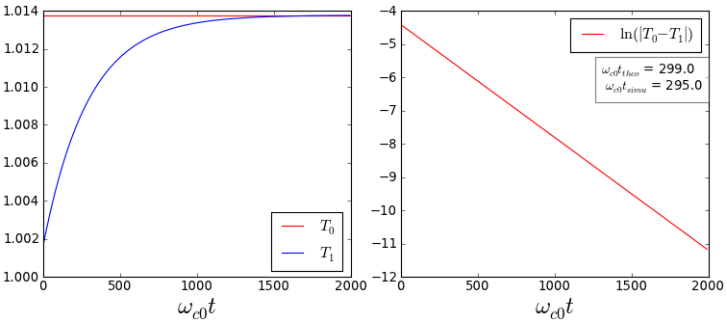

4.2. Neoclassical test

The intrinsic properties of the collision operator reported in the previous section are mandatory but relatively easy to satisfy. A more challenging test is provided by neoclassical theory. For the single species case, the poloidal rotation and heat diffusion coefficient can be compared with theoretical predictions in a pure axisymmetric case, i.e. without any instability. For the two species case, the radial flux of a trace impurity is compared with the neoclassical prediction. These tests allow one to test, different parts of the collision operator depending on the collisionality regime and the number of species. These tests are useful as the results are sensitive to the details of the collision operator.

4.2.1. Neoclassical validation in the single species case

The neoclassical theory is tested by filtering out non axisymmetric components of the electrical potential. Especially, this filtering removes turbulence. Four simulations are performed with a scan in $\nu_\star$ going from 10^{-2} to 10. The phase space grid used for these simulations is $\left(r, \theta, \phi, v_\parallel, \mu\right) = (256, 256, 32, 128, 64)$. The dimension of the tokamak that is simulated is fixed by $\rho_\star = 150$ and the inverse aspect ratio $\epsilon = 0.31$ at midradius. The collisionnal time step depends on $\nu_\star$ and the numerical time step is adapted consistently to keep the same temporal resolution of collisions. In the single species neoclassical theory, two quantities are of utmost importance : the poloidal rotation and heat diffusivity. These two quantities are

compared with theoretical predictions to validate GYSELA's operator.

In neoclassical theory, the poloidal velocity is tied to the thermal gradient by the relation $v_\theta = k_{neo}(\nu_\star, \epsilon)\frac{\nabla T}{eB}$. Theoretical predictions of k_{neo} are accurate in the banana and Pfirsch-Schlüter regimes and approximate in the plateau regime. The sign of the poloidal velocity is expected to depend on the collisionality regime : rotation in the the ion diamagnetic direction ($k_{neo} > 0$) is expected in the banana regime and the opposite ($k_{neo} < 0$) in the Pfirsch-Schlüter regime. The transition is expected to take place in the plateau regime. A model inspired from Hirshman Sigmar is given by Kim [14] and predicts k_{neo} in all collisionality regimes including corrections due to finite aspect ratio ϵ. This theoretical prediction is used to benchmark GYSELA's operator. The results are shown in figure (8). The shape of the curve is the same and the inversion of sign takes place in the plateau regime as expected by theory. The agreement is better for the banana regime where the theoretical prediction is more accurate.

Another important quantity predicted by neoclassical theory is the thermal diffusion coefficient χ_{neo}. Even if neoclassical transport is subdominant as compared to the turbulent one for the main species, it can be important for heavy impurities like tungsten and for the main species close to transport barriers where turbulent transport is reduced. To check their validity, GYSELA results are compared with the Chang-Hinton prediction [4] valid in all collisionality regimes . The results are shown in the figure (9). Again a satisfactory agreement with analytical prediction is found.

Figure 8: Comparison of k_{neo} predicted by theory with GYSELA results

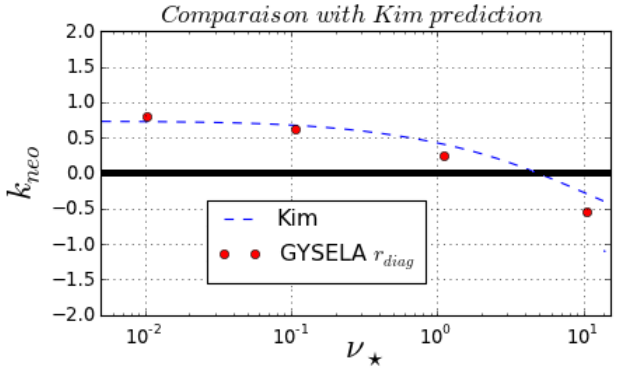

Figure 9: Comparison of χ_{neo} predicted by theory with GYSELA results

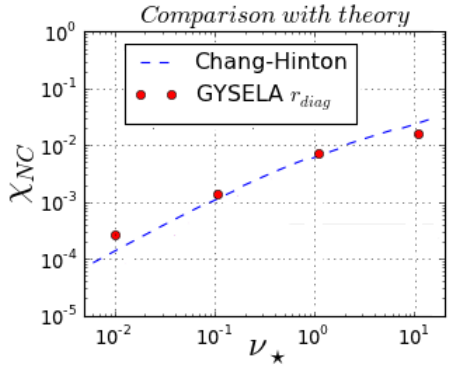

4.2.2. Neoclassical validation in the two species case

Neoclassical transport is expected to be dominant for heavy impurities. In this framework, the following tests are performed for tungsten as the second species in the trace limit ($\alpha = \frac{n_z Z_z^2}{n_i Z_i^2} \ll 1$) for simplicity. In fusion plasmas, tungsten is only partially stripped and its ionization state should depends on the spatial location. But only one charge state is allowed in the current version of the GYSELA code. Thus a fixed charge is chosen for the tungsten $Z_W = 40$. The main species is deuterium in the banana regime $\nu_D^\star = 0.1$. Tungsten is therefore in the Pfirsch Schlüter regime as $\nu_W^\star \simeq \sqrt{2} Z_W^2 \sqrt{\frac{m_D}{m_W}} \nu_D^\star \simeq 236 \nu_D^\star = 23,6$.

A derivation of the theoretical prediction for trace impurity transport in the Pfirsch-Schlütter regime can be found in [12]. We recall here only the main steps. The starting point is to link the radial flux of particles to the collisional friction force. The easiest way to do it is to use the toroidal momentum conservation equation for species s

$$\partial_t L_{\varphi,s} + \partial_\psi \Pi^\Psi_{\varphi,s} = Ze\left(\Gamma^\Psi_s - \Gamma^\Psi_{E,s}\right) + \left\langle \frac{I}{B} R_{\parallel,s} \right\rangle_\Psi$$

with

$$L_{\varphi,s} = m_s \int d\tau u_\varphi F_s$$

$$\Pi^\Psi_{\varphi,s} = m_s \int d\tau u_\varphi F_s v^\Psi$$

$$\Gamma^\Psi_{E,s} = \int d\tau F_s \partial_\varphi \bar{\phi}$$

$$\Gamma^\Psi_s = \int d\tau F_s v^\Psi = \langle \boldsymbol{\Gamma}_{\perp,s} \cdot \nabla\Psi \rangle_\Psi$$

Where $u_\varphi = \frac{I}{B} v_\parallel$ and $\bar{\phi}$ is the gyro-averaged electric potential Here $d\tau = d^3\boldsymbol{v} \frac{d\theta d\varphi}{\boldsymbol{B}\cdot\nabla\theta}$ is the phase space volume element in between two magnetic surfaces Ψ and $\Psi + d\Psi$ and $\langle ... \rangle_\Psi$ indicates the flux surface average. $R_{\parallel,s}$ is the total collisional drag force $R_{\parallel,s} = \sum_{s'} R_{\parallel,ss'}$ which is linked to the $V_{\parallel i}$ and $q_{\parallel i}$ via the equation (6). Finally these parallel quantities can be linked to radial gradients of densities and temperature in two steps. The first step consists in linking the perpendicular components of velocity $V_{\perp i}$ and heat flux $q_{\perp i}$ to the gradients of densities and temperature. Neglecting poloidal asymmetries, one can show that

$$\boldsymbol{V}_{\perp i} = \frac{\boldsymbol{B}\times\nabla\Psi}{B^2}\omega_i(\Psi) \text{ where } \omega_i(\Psi) = \frac{1}{n_i Z_i e}\frac{\partial p_i}{\partial \Psi} + \frac{\partial \phi}{\partial \Psi}$$

$$\boldsymbol{q}_{\perp i} = \frac{5}{2}\frac{p_i}{Z_i e B^2}\frac{\partial T_i}{\partial \Psi}\boldsymbol{B}\times\nabla\Psi \tag{9}$$

Then assuming stationary flows, one can use the incompressibility of the flow ($\nabla(n\boldsymbol{V}) = 0$) and the incompressibility of the heat flux ($\nabla \boldsymbol{q} = 0$) to link the perpendicular components to the parallel ones:

$$V_{\parallel i} = \frac{\langle B V_{\parallel i}\rangle_\Psi B}{\langle B^2\rangle_\Psi} - \omega_i(\Psi) I(\Psi)\left(\frac{1}{B} - \frac{B}{\langle B^2\rangle_\Psi}\right)$$

$$q_{\parallel i} = \frac{\langle B q_{\parallel i}\rangle_\Psi B}{\langle B^2\rangle_\Psi} - \frac{5}{2}\frac{p_i}{Z_i e}\frac{\partial T_i}{\partial \Psi} I(\Psi)\left(\frac{1}{B} - \frac{B}{\langle B^2\rangle_\Psi}\right) \tag{10}$$

Then using eq.(6) one can compute the parallel exchange of momentum between species due to collisions

$$R_{\|zi} = \nu_{zi}\frac{m_z T_{z,eq} I}{Ze}\left(\frac{1}{B}-\frac{B}{\langle B^2\rangle_\Psi}\right)n_{z,eq} \times \left[\frac{\partial \ln n_{z,eq}}{\partial\Psi}-\frac{Z_z}{Z_i}\frac{\partial \ln n_{i,eq}}{\partial\Psi}-H_{theo}\frac{Z_z}{Z_i}\frac{\partial \ln T_{eq}}{\partial\Psi}\right]$$

where the contribution of parallel heat flux of the impurity has been dropped due the mass ratio between impurity and the main species. Then putting all together, and noticing that all terms which do not involve radial gradients cancel out in virtue of parallel force balance, one recovers the usual expression for impurity flux due to neoclassical physics

$$\Gamma_z = -n_Z D_{theo}\left[\frac{\nabla n_z}{n_z}-Z\frac{\nabla n_i}{n_i}-H_{theo}Z\frac{\nabla T}{T}\right]$$

Where Γ_z is a modified impurity flux

$$\Gamma_z = \frac{dr}{d\Psi}\left[\Gamma_z^\Psi-\Gamma_{E,z}^\Psi-\frac{1}{Z_z e}\left(\partial_t L_{\varphi,z}+\partial_\psi \Pi_{\varphi,z}^\Psi\right)\right]$$

It is often assumed that $\Gamma_z \simeq \frac{dr}{d\Psi}\Gamma_z^\Psi = \langle \mathbf{\Gamma}_{\perp,z}\cdot\nabla r\rangle_\Psi$. But in the simulations, the contribution of the other terms are non-vanishing and they need to be taken into account for a precise comparison between simulation and theoretical prediction.

Recovering the expected neoclassical expression of the thermal screening coefficient H_{theo} reveals as a stringent test of both the Vlasov part (the left hand side of the gyrokinetic equation, governing the trajectories) and the collision operator. More precisely, the final value – and sign – of H_{theo} results from a partial compensation between two different contributions: the one coming from the parallel velocities of both species ($\simeq 1$), and the other one coming from the parallel heat flux of the main ions $\left(\simeq -\frac{3}{2}\right)$.

In this framework, the accurate computation of $q_{\|i}$ is a critical issue. As a matter of fact, its neoclassical expression eq.(10) results from the incompressibility of the total flux $\nabla\cdot q_i = 0$. The transverse flux $q_{\perp i}$ computed in GYSELA is in perfect agreement with the neoclassical prediction, eq.(9). Conversely, the present accuracy of the energy balance does not reveal sufficient to recover the expected expression of $q_{\|i}$: while the poloidal shape is properly recovered, the magnitude is not. Ongoing efforts are conducted to solve this issue. Notice however that this issue *is not* related to the collision operator, although it impacts neoclassical transport. Indeed, it deals with the treatment of the Vlasov part of the gyrokinetic equation. For the time being, the solution to overcome this difficulty is to impose that the parallel heat flux takes the expected value eq.(10) in the collision operator. This has been used to get the following results.

The diffusion coefficient and the screening factor in the Pfirsch-Schlütter regime with trace impurities are given respectively by $D_{theo} = 2q^2\rho_i^2\nu_{iz}/\alpha$ and $H_{theo} \simeq -0.5 + 0.29/\left(0.59+1.34g^{-2}\right)$ with $g=\nu_i^\star\epsilon^{3/2}$ [12]. To test this prediction we assume that the flux computed in GYSELA takes the general form

$$\Gamma_z^{gys} = -n_Z D_{gys}\left[\frac{\nabla n_z}{n_z}-K_{gys}Z\frac{\nabla n_i}{n_i}-H_{gys}Z\frac{\nabla T}{T}\right]$$

Then one only needs to determine D_{gys}, K_{gys} and H_{gys} and to compare them with their analytical prediction D_{theo}, 1 and H_{theo} . To do so, two simulations are used. The first one with $\nabla T \simeq 0$ is used to compute D_{gys} and K_{gys}. Radial density profiles are chosen to get a radial scan of $\frac{\nabla n_z}{n_z}(\rho) - Z\frac{\nabla n_i}{n_i}(\rho)$ around zero. Recording $\Gamma_z/n_z(\rho)$, it is possible to plot Γ_z/n_z as a function of $\frac{\nabla n_z}{n_z}-Z\frac{\nabla n_i}{n_i}$, using the global character of GYSELA and the local behaviour of neoclassical transport. The result of this simulation is given in fig.10. The good linear fit gives confidence in the dependence of the flux of tungsten on the density gradients of both species. The discrepancy with the theoretical prediction for K_{gys} is of few percents and the one on the diffusion coefficient D_{gys} is below 15%.

Figure 10: Measurement of D_{gys} and K_{gys}

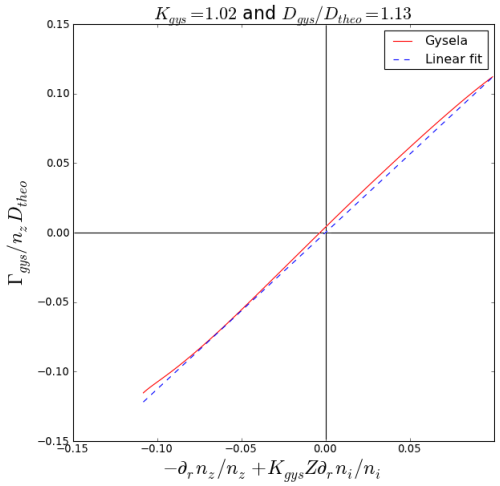

The second step consists in a simulation with $\frac{\nabla n_z}{n_z}-Z\frac{\nabla n_i}{n_i}=0$. In this case the flux is expected to be directly proportional to the temperature gradient $\Gamma_z = -n_Z D_{gys}H_{gys}Z\frac{\nabla T}{T}$ as the previous simulation has shown that $K_{gys}\simeq 1$. Using also the fact that the diffusion coefficient is close to the theoretical prediction, we can replace D_{gys} by D_{theo} in the previous expression and then directly measure H_{gys} using a method similar to the one presented previously. The result is given in fig.11. Again a discrepancy of few percent is found between results from the code and theoretical prediction.

Figure 11: Measurement of the screening factor H_{gys}

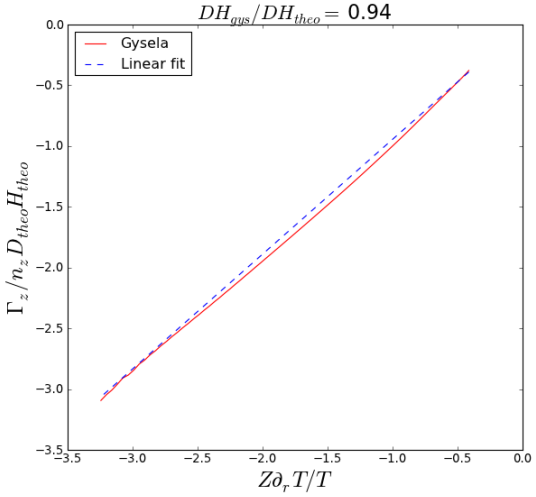

4.3. Zonal flow damping

Zonal flows are known to control the level of turbulence by tearing apart vortices [6]. The main damping mechanism for these flows comes from collisional friction. It is then critical to get the correct damping rate of zonal flows to predict the right level of turbulence. Collisionless plasmas are known to exhibit linearly undamped axisymmetric ϕ_{00} [16]. Hinton and Rosenbluth [11] have predicted the collisional damping of this residual flow.

$$\begin{aligned}\frac{\phi_{00}(t)}{\phi_{00}(t=0)} &= \exp\left(\frac{\beta^2}{\alpha^2}t\right)\operatorname{erfc}\left(\frac{\beta}{\alpha}\sqrt{t}\right) \\ &+ \operatorname{erf}(\nu_0 t)\,\alpha\frac{B_\theta^2}{B^2}\left[\begin{array}{c} 1.8\,(\nu_0 t)^{5/9}\exp\left(-(3\nu_0 t)^{2/3}\right) \\ +1+\frac{1.4}{\epsilon}\exp(-\nu_d t)\end{array}\right]\end{aligned}$$

Where $\alpha = 1 + 1.6\frac{q^2}{\sqrt{\epsilon}}$ is the collisionless residual, $\beta = \frac{3\pi q^2 \bar{\nu}^{1/2}}{\epsilon\Lambda^{3/2}}$, $\Lambda = \lambda \ln\left(16\left(\frac{\epsilon}{\bar{\nu}t}\right)^{1/2}\right)$ with $\lambda \simeq 1$ and some frequencies associated with collisions are defined as $\bar{\nu} = 0.61\nu_{ii}$, $\nu_0 = 1.9\nu_{ii}$, $\nu_d = \frac{\nu_{ii}}{0.64\sqrt{\epsilon}}$. The initial time corresponds to the case where all GAM oscillations have been Landau damped. Details on GAM oscillation and damping can be found in the literature [20, 17]. The first term corresponds to the fast collisional smoothing of the distribution function in the trapping boundary layer. The last term is the contribution from high-energy ions which have small collision frequencies and thus dominate the long time behaviour. An extra term $\operatorname{erf}(\nu_0 t)$ has been added in front of the last term of the right hand side to ensure the relation also holds for initial time.

The collisional damping of the residual can be tested by first launching a collisionless simulation, waiting for GAM damping and then adding collisions. A good agreement is found between predicted and computed ϕ_{00} decay once collisions are activated as can be seen in figure 12. To have a better match, the value of λ has been adjusted ($\lambda = 1.04$).

Figure 12: Collisional damping of ϕ_{00}

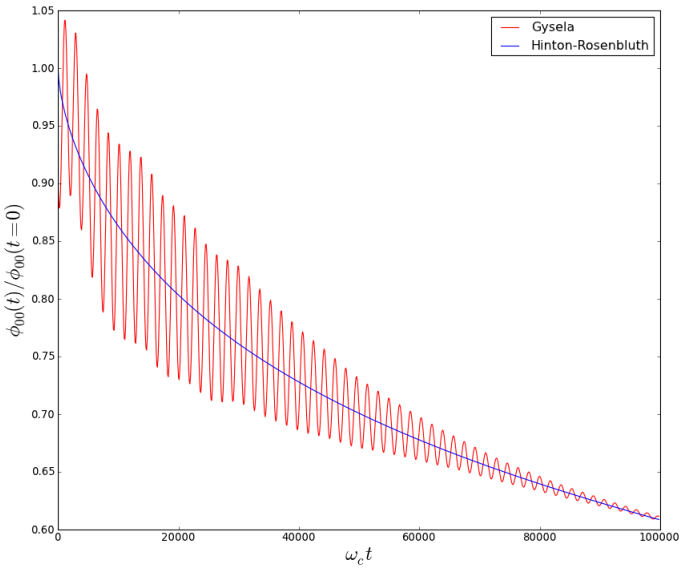

5. Conclusion

A new multi-species collision operator has been implemented and tested in the gyrokinetic code GYSELA. It is valid for species of arbitrary mass and charge. It is peculiar as it acts directly in the $(v_\parallel, \mu)$ set of coordinates. The main properties have been tested successfully. Firstly the intrinsic properties of the operator have been validated : conservation properties, exchange rates, relaxation to the Maxwellian. Secondly, the neoclassical physics for single and two species have been been compared successfully with theoretical predictions. These tests are sensitive to details of the collision operator and thus give a set of stringent criterion to test any collision operator. Finally the collisional damping of zonal flows has been recovered.

This new collision operator allows the GYSELA code to study more accurately trapped electron modes turbulence which have been recently added to the code. Moreover, it allows one the study of multi-species plasmas with no restriction on the relative concentration between species.

Aknowledgements

This work was granted access to the national HPC ressources of OCCIGEN/CINES and European machine dedicated to fusion Marconi/CINECA. This work has been carried out within the framework of the EUROfusion Consortium and has received funding from the Euratom research and training programme 2014-2018 under grant agreement No 633053 for the project WP17-ENR-CEA-02. The views and opinions expressed herein do not necessarily reflect those of the European Commission.

Appendix : Numerical aspects

In this appendix, we detail the choice of the main numerical parameters used for the collision operator. The first step is the number of polynomials N_{pol} kept for the projection in the μ direction. For this choice, the most stringent test is to retrieve k_{neo} in the single species case. The minimal number of polynomials to have the expected poloidal rotation is $N_{pol} = 3$. Once the number of polynomials is set, one has to choose the discretization in the μ direction. A necessary condition for the projection to work properly is to ensure the orthogonality of the polynomials and so to check the condition

$$\left\| \delta_{ij} - \int du e^{-u} P_i(u) P_j(u) \right\| \ll 1 \text{ for any i,j}$$

One can show that the optimal choice for the number of points in the μ direction is $N_\mu = 64$ and the optimal value for the the upper limit in the μ direction is $\mu_{max} \simeq \frac{16T}{B}$. The number of points in the $v_\parallel$ direction is less critical in terms of numerical cost. 128 points reveal sufficient for the collision operator.

The last point is to choose the collisional time step Δt_{coll}. Indeed in order to save computational ressource, the collision operator can be used on a different time scale as the the rest of the code GYSELA. Of course, the collisional time step Δt_{coll} has to be proportional to $(\max(\nu_s^\star))^{-1}$where $\nu_s^\star$ is the collisionality of the s species .

References

[1] Abel, I. G., Barnes, M., Cowley, S. C., Dorland, W., & Schekochihin, A. A. 2008. Linearized model Fokker-Planck collision operators for gyrokinetic simulations. I. Theory. *Physics of Plasmas*, **15**(12), 122509.

[2] Barnes, M., Abel, I. G., Dorland, W., Ernst, D. R., Hammett, G. W., Ricci, P., Rogers, B. N., Schekochihin, A. A., & Tatsuno, T. 2009. Linearized model Fokker-Planck collision operators for gyrokinetic simulations. II. Numerical implementation and tests. *Physics of Plasmas*, **16**(7), 072107.

[3] Brizard, Alain J. 2004. A guiding-center Fokker-Planck collision operator for nonuniform magnetic fields. *Physics of Plasmas*, **11**(9), 4429–4438.

[4] Chang, C. S., & Hinton, F. L. 1986. Effect of impurity particles on the finite aspect ratio neoclassical ion thermal conductivity in a tokamak. *The Physics of Fluids*, **29**(10), 3314–3316.

[5] Crank, J., & Nicolson, P. 1996. A practical method for numerical evaluation of solutions of partial differential equations of the heat-conduction type. *Advances in Computational Mathematics*, **6**(1), 207–226.

[6] Diamond, P H, Itoh, S-I, Itoh, K, & Hahm, T S. 2005. Zonal flows in plasmas - a review. *Plasma Physics and Controlled Fusion*, **47**(5), R35.

[7] Estève, D., Garbet, X., Sarazin, Y., Grandgirard, V., Cartier-Michaud, T., Dif-Pradalier, G., Ghendrih, P., Latu, G., & Norscini, C. 2015. A multi-species collisional operator for full-F gyrokinetics. *Physics of Plasmas*, **22**(12), 122506.

[8] Estève, D., Sarazin Y. Garbet X. Grandgirard V. Breton S. Donnel P. Asahi Y. Bourdelle C. Dif-Pradalier G. Ehrlacher C. Emeriau C. Ghendrih P. Gillot C. Latu G. Passeron C. 2017. Self-consistent gyrokinetic modeling of neoclassical and turbulent impurity transport. *Nuclear Fusion*.

[9] Grandgirard, V., Abiteboul, J., Bigot, J., Cartier-Michaud, T., Crouseilles, N., Dif-Pradalier, G., Ehrlacher, Ch., Esteve, D., Garbet, X., Ghendrih, Ph., Latu, G., Mehrenberger, M., Norscini, C., Passeron, Ch., Rozar, F., Sarazin, Y., SonnendrÃŒcker, E., Strugarek, A., & Zarzoso, D. 2016. A 5D gyrokinetic full-f global semi-Lagrangian code for flux-driven ion turbulence simulations. *Computer Physics Communications*, **207**, 35 – 68.

[10] Hinton, F. L., & Hazeltine, R. D. 1976. Theory of plasma transport in toroidal confinement systems. *Rev. Mod. Phys.*, **48**(Apr), 239–308.

[11] Hinton, F L, & Rosenbluth, M N. 1999. Dynamics of axisymmetric EXB and poloidal flows in tokamaks. *Plasma Physics and Controlled Fusion*, **41**(3A), A653.

[12] Hirshman, S, & Sigmar, D.J. 1981. Neoclassical transport of impurities in tokamak plasmas. **21**(01), 1079.

[13] Hirshman, S. P., & Sigmar, D. J. 1976. Approximate Fokker-Planck collision operator for transport theory applications. *The Physics of Fluids*, **19**(10), 1532–1540.

[14] Kim, Y. B., Diamond, P. H., & Groebner, R. J. 1991. Neoclassical poloidal and toroidal rotation in tokamaks. *Physics of Fluids B: Plasma Physics*, **3**(8), 2050–2060.

[15] Manas, P., Camenen, Y., Benkadda, S., Hornsby, W. A., & Peeters, A. G. 2015. Enhanced stabilisation of trapped electron modes by collisional energy scattering in tokamaks. *Physics of Plasmas*, **22**(6), 062302.

[16] Rosenbluth, M. N., & Hinton, F. L. 1998. Poloidal Flow Driven by Ion-Temperature-Gradient Turbulence in Tokamaks. *Phys. Rev. Lett.*, **80**(Jan), 724–727.

[17] Sugama, H., Watanabe, T.-H., & Nunami, M. 2009. Linearized model collision operators for multiple ion species plasmas and gyrokinetic entropy balance equations. *Physics of Plasmas*, **16**(11), 112503.

[18] T. Görler, X. Lapillonne, S. Brunner T. Dannert F. Jenko F. Merz, & Told, D. 2011. The global version of the gyrokinetic turbulence code GENE. *Journal of Computational Physics 230, 7053.*

[19] Vernay, T., Brunner S. Villard L. Mcmillan B. Sauter O. Jolliet S. Tran T.M. Bottino A. 2012. Global Collisional Gyrokinetic Simulations of ITG Microturbulence Starting from a Neoclassical Equilibrium. **260**(12), 012021.

[20] Zonca, F., & Chen, L. 2008. Radial structures and nonlinear excitation of geodesic acoustic modes. *EPL (Europhysics Letters)*, **83**(3), 35001.